Long Wave Infrared Type II Superlattice Focal Plane Array Detector

P.C. Klipstein[*], E. Avnon, Y. Benny, A. Fraenkel, A. Glozman, E. Hojman, E. Ilan,
E. Kahanov, O. Klin, L. Krasovitski, L. Langof, I. Lukomsky, M. Nitzani, L. Shkedy,
I. Shtrichman, N. Snapi, R. Talmor, A. Tuito, S. Vaserman, and E. Weiss

SemiConductor Devices, P.O. Box 2250, Haifa 31021, Israel
[*]*E-mail: philip_k@scd.co.il*

ABSTRACT

The XBn/XBp family of barrier detectors enables diffusion limited dark currents comparable with Hg$_x$Cd$_{1-x}$Te Rule-07 and high quantum efficiencies. SCD's XBp type II superlattice (T2SL) detector contains InAs/GaSb and InAs/AlSb T2SLs, and was designed for the long wave infrared (LWIR) atmospheric window using $\mathbf{k \cdot p}$ based modelling of the energy bands and photo-response. Wafers are grown by molecular beam epitaxy and are fabricated into focal plane array (FPA) detectors using standard FPA processes, including wet and dry etching, indium bump hybridisation, under-fill, and back-side polishing. The 640×512 pixel, 15 μm pitch, detector goes by the name of 'Pelican-D LW' and exhibits a quantum efficiency of ~ 50 per cent with background limited performance at an operating temperature of 77 K. It has a cut-off wave length of ~ 9.5 μm, with a pixel operability of above 99 per cent. The detector gives a very stable image with a residual non uniformity of below 0.04 per cent over its useful dynamic range. A new digital read-out integrated circuit has been designed so that the complete detector closely follows the configuration of SCD's MWIR Pelican-D detector.

Keywords: Long Wave Infrared; LWIR; Superlattice; Type II superlattices; Focal plane array

ABBREVIATIONS

AL	Active layer
ARC	Anti reflection coating
BL	Barrier layer
BLIP	Background limited performance
CL	Contact layer
DDC	Detector-dewar-cooler
FPA	Focal plane array
G-R	Generation-recombination
Hg$_x$Cd$_{1-x}$Te	Mercury cadmium telluride
IDCA	Integrated dewar cooler assemblies
LWIR	Long-wave-infrared
MBE	Molecular beam epitaxy
MWIR	Mid-wave-infrared
NETD	Noise equivalent temperature difference
NUC	Non uniformity correction
QE	Quantum efficiency
ROIC	Read out integrated circuit
RNU	Residual non uniformity
SRH	Shockley-Read-Hall
T2SL	Type II superlattice
WF	Well fill
1PC	One point correction
2PC	Two point correction

1.   INTRODUCTION

Type II superlattices (T2SLs) based on thin layers of InAs and GaSb bear a close relationship with the alloy, Hg$_x$Cd$_{1-x}$Te, where the bandgap vanishes at a critical value of the composition parameter, x. In T2SLs, the bandgap vanishes when the layer thicknesses are beyond a critical value. Hg$_x$Cd$_{1-x}$Te has become one of the most widely used tunable infrared detector materials, because it is a versatile technology that can match the characteristic photon wavelength of most infrared applications. On the other hand, T2SLs have only recently been considered to be a viable alternative technology to Hg$_x$Cd$_{1-x}$Te, due to the more challenging crystal growth that is required. T2SLs must be grown by molecular beam epitaxy (MBE), which has taken longer to mature to a viable commercial production tool than the liquid phase epitaxy technique that is used most widely in the production of Hg$_x$Cd$_{1-x}$Te detector arrays. An important factor driving T2SL development, however, is that commercial 3″ or 4″ GaSb substrates can be used for their growth, while smaller and more expensive CdZnTe substrates must be used for the highest quality Hg$_x$Cd$_{1-x}$Te.

Yet two more technological hurdles still had to be overcome, before T2SL technology began to look truly competitive. The first was the suppression of generation-recombination (G-R) limited dark current[1], which is absent in high quality Hg$_x$Cd$_{1-x}$Te photodiodes, and the second was device passivation. A novel barrier device, known as an XBp

135

detector[2,3], was developed at SCD, which contains two types of T2SL: InAs/GaSb for the photon absorbing or 'active' layer and InAs/AlSb for the barrier layer. All T2SLs are doped p-type which ensures that the depletion layer is confined to the wide bandgap barrier layer. Figure 1(a) shows a schematic diagram of the T2SL band structure. In Fig. 1(b) the edges of the mini-bands shown in (a) are sketched for an operating pB_pp device, which is one of the four possible configurations of an XBp detector[4]. Note that this is a unipolar device where all layers are doped p-type. G-R current occurs in the depleted barrier layer through mid-gap Shockley-Read-Hall (SRH) traps with an activation energy close to half of its bandgap. Since this bandgap is more than twice that of the active layer, the G-R current is negligible compared to the diffusion current coming out of the active layer. For this current, the activation energy is equal to the full active layer bandgap, since all SRH traps are occupied[4]. In this work it will be shown that the dark current in a T2SL XBp device is quite close to the Rule 07 value, which is the state of the art metric for $Hg_xCd_{1-x}Te$ photodiodes[5].

The second technological hurdle that had to be overcome was a reliable passivation treatment of the processed XBp devices, which is compatible with all of the standard FPA processes, including wet and dry etching, indium bump hybridisation, glue under-fill, and back-side polishing. The development of this passivation at SCD is the final step that has enabled the fabrication of long wave infrared (LWIR) T2SL FPAs with a performance comparable to high quality $Hg_xCd_{1-x}Te$ FPAs. The design and performance of these FPAs is the subject of this study.
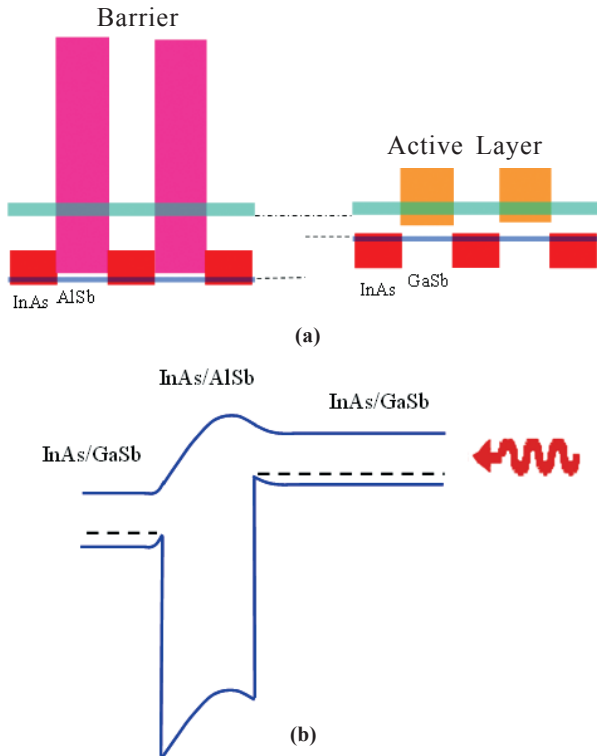

Figure 1. (a) Alignment between mini-bands in the active and barrier layers of a T2SL XBp device, superimposed on the band gaps of InAs, GaSb and AlSb (b) Schematic profile of band edges in an operating pB_pp device, based on the mini-bands shown in (a).

2. DESIGN AND PERFORMANCE OF T2SL BARRIER DEVICES

The advantage of the barrier device is demonstrated in Fig. 2, which compares a standard LWIR n-on-p diode based solely on InAs/GaSb and operating at a bias of 0.1V, with a LWIR pB_pp device based on the design in Fig. 1, and operating at a bias of 0.6 V. Both devices have an active layer band gap wavelength close to 10 μm. The barrier device (blue line) is diffusion limited down to 77 K, while the diode (red line) is G-R limited at this temperature, with a dark current over 20× larger. The dark current in the barrier device of Fig. 2 and in all of our XBp test devices is only about one order of magnitude larger than the $Hg_xCd_{1-x}Te$ Rule-07 value[6].
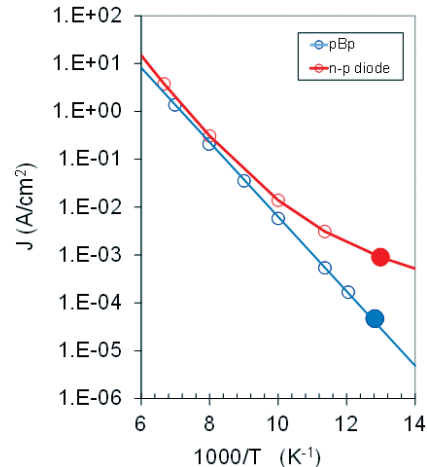

Figure 2. Log J_{dark} vs. 1000/T in pB_pp barrier device (bias = 0.6V) and n-p diode (bias = 0.1V), each with an InAs/GaSb active layer bandgap wavelength of λ_G~10 μm (mesa area = 100×100 μm²).

We are able to simulate the full spectral response of an FPA made from the pB_pp device shown in Fig. 1, if the thicknesses of the InAs and GaSb layers in the T2SL period are known. This allows us to design the superlattices inside the structure correctly, prior to MBE growth. The simulation is based on a $k \cdot p$ treatment and optical transfer matrix (OTM) calculation recently reported elsewhere[7]. While the OTM technique is fairly standard, the $k \cdot p$ treatment contains a number of innovations[8]. This treatment leads to a reduced number of fitting parameters compared to other approaches, namely two independent Luttinger parameters (of InAs), three interface parameters, the valence band offset and a parameter close to unity that is related to the interband momentum matrix element. The same two Luttinger parameters are used for all superlattices of the form InAs/X where X = GaSb or AlSb, so they only need to be determined once. The fitted values turn out to be very close to those determined by other workers. All other parameters used in the calculation are based on established spectroscopic, mechanical or X-ray data available in the literature.

Figure 3 shows an OTM calculation of the spectral response of a pB_pp detector with an antireflection coating (ARC) and a 4.5 μm thick AL based on a 13.8/7 InAs/GaSb T2SL with a cut-off wavelength close to 10 μm. The OTM calculation uses a T2SL absorption spectrum deduced from the $k \cdot p$ model. Although the InAs/AlSb barrier layer makes
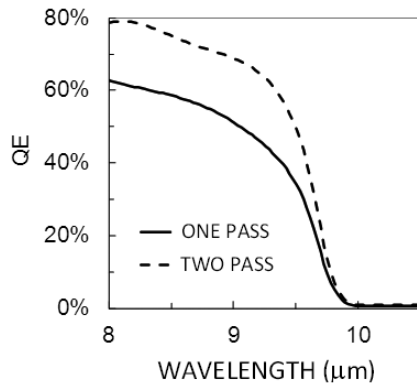
Figure 3. **Calculated spectral response (quantum efficiency) for a XB$_p$p detector with a 4.5 µm thick AL made from a 13.8/7 InAs/GaSb T2SL when none of the LWIR radiation (solid line) or 80 per cent of the LWIR radiation (dashed line) is reflected back from the contact for a second pass through the AL.**

no contribution to the detector response, the **k · p** treatment described above is also used to design the correct layer widths in the barrier layer of the grown device. Figure 3 shows curves for both a single pass device (solid line) and a two pass device (dashed line) in which 80 per cent of the light impinging on the metal contact of the contact layer is reflected back for a second pass through the active layer. It has been assumed that there are no losses of photo-carriers due to recombination in the bulk or at the surfaces (internal QE = 100 per cent). Under these conditions, the two pass detector is able to provide an average QE of ~ 65 per cent, defined as the spectral response in Fig. 3 weighted by the 300 K black body radiation spectrum and averaged from the cut-on of the LWIR atmospheric widow (~ 8 µm) to the detector cut-off wavelength. The corresponding value for the single pass device is ~ 50 per cent. It is shown in the subsequent paras that the single pass value can be realised in a FPA which was designed as a one pass detector.

3. 640 × 512/15 MICRON DIGITAL ROIC

The new ROIC has an architecture that closely follows that of the mature and successful MWIR Pelican D ROIC[9]. This approach was chosen due to the excellent performance expected in terms of readout noise, Residual Non Uniformity (RNU), power dissipation and frame rate. Another important incentive was to support our incumbent customers with fast integration into systems and cameras. Nevertheless, the new T2SL LWIR technology poses two important challenges for the ROIC design:

1. The device polarity requires a polarity inversion in the ROIC circuitry.
2. The higher photon flux compared with the MWIR imposes very short integration periods due to the limited area available for the integration capacitors

To overcome this problem we have implemented a high frame rate (up to 360 Hz) with frame averaging (up to 8 frames) performed in the proximity electronics. This enables us to achieve an NETD value @ F/2.7 and 30 Hz of less than 15 mK.

The ROIC was tested at room temperature and 77 K and

the results compared favourably with preliminary predictions. Table 1 presents the measured performance.

Table 1. Pelican-D LW ROIC performance at 77 K

Parameter	Value
Well capacity	> 6 Me⁻
Noise floor	< 1300 e⁻
ROIC RNU	< 0.025 per cent of DR
Dynamic range	5350
ADC resolution	13 bit (> 7000 DL)
Maximum frame rate	360 Hz
Input clock frequency	80 MHz
Power consumption	110 mW @ 360Hz
Windowing	Supported
Up/down readout	Supported
Integration modes	ITR, IWR

4. PELICAN-D LW FPA

'Pelican-D LW' is the first in our new line of LWIR XBp FPAs manufactured at SCD. The detector is based on a 15 µm pitch, 640 × 512 FPA bonded to the new digital silicon ROIC, as described in the previous para. The FPA has a nominal T2SL cut-off wavelength of 9.5 µm. In the rest of this section, we present some of its key radiometric performance parameters. Dark current, QE, and NETD were measured at 77 K in a laboratory test Dewar, for this FPA, and in the case of dark current, for several others with different cut-off wavelengths. Residual non-uniformity (RNU) and an example of a real image, however, were measured after final integration of the FPA into a Detector-Dewar-Cooler (DDC) assembly.

Figure 4 shows the FPA dark current distribution at 77K for 5 FPAs with cut-off wavelengths spanning the nominal value of 9.5 µm. The median value for a cut-off of 9.4 µm is close to 100 pA and the distribution is quite narrow with a full width at half maximum of only ~6 per cent of the median. The maximum distribution width is 12 per cent, for the two FPAs with a 9.8 µm cut-off, which is still quite narrow. Note that these two FPAs have virtually identical distributions, showing the high reproducibility of our FPA process. None of the distribution curves have a significant high current tail, and their narrow widths demonstrate a high degree of uniformity. A narrow dark current distribution is very good for the stability of the FPA against temperature or bias fluctuations. The median dark current values of all five FPAs are about one order of magnitude greater than the dark current range predicted by $Hg_xCd_{1-x}Te$ Rule-07[5].

Our T2SL FPA technology leads to a remarkably uniform signal before any non-uniformity correction (NUC) has been performed, with no stains or large clusters of defective pixels. This leads to a very small RNU after a two point NUC (2PC) is performed. The magenta line in Fig. 5 shows a plot of RNU *vs.* well fill (WF) for an FPA at 77 K, measured using different black body temperatures and a constant integration time, with a 2PC performed at WF values of 52 per cent and 72 per cent respectively. The RNU remains below 0.02 per cent of the dynamic range for WF values in the range 40 per cent - 80
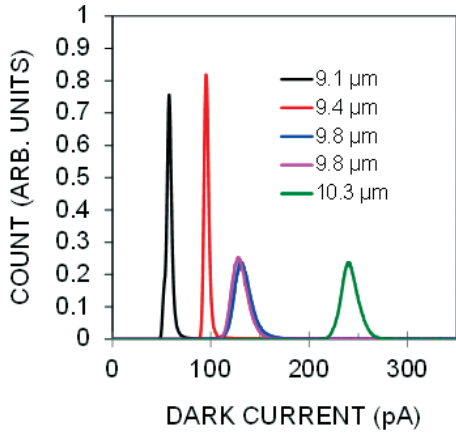
Figure 4. 77 K dark current distribution of five Pelican-D LW FPAs with cut-off wavelengths between 9.1 µm and 10.3 µm (normalised to constant area).
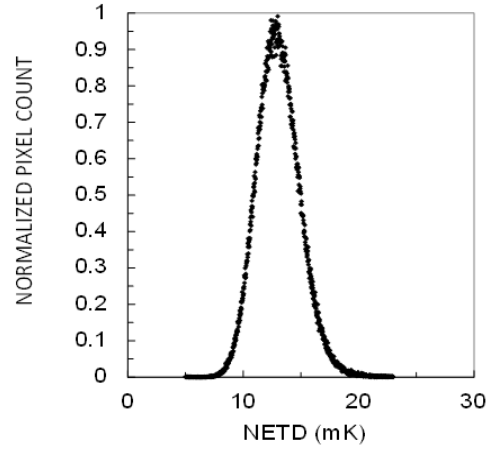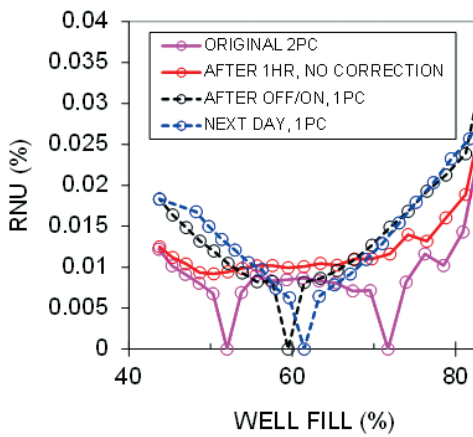

Figure 5. RNU of Pelican-D LW FPA at 77 K after performing a two point correction (2PC) at 54 per cent and 72 per cent well fill (magenta); one hour later with no correction (red); After turning off and on with a 1PC (black dash); Next day with a 1PC (blue dash).

per cent. Moreover, the FPA is very stable and can maintain a stable image for many hours without any further corrections, as shown by the red line, which was registered one hour after the 2PC was performed. The dashed lines show RNU curves after switching the detector off and then immediately back on (black), or back on the next day (blue), and performing a 1PC. In all cases the RNU curves remain within ~0.01 per cent of the original calibration curve.

At 65 per cent well fill of its 6 Me⁻ capacitor and a frame rate of 240 Hz, Pelican-D LW offers an NETD of 36 mK when configured with F/2.7 optics. By averaging 8 frames at a time, the detector operates at an effective frame rate of 30 Hz. The NETD distribution measured under these conditions for the Pelican-D LW FPA is as shown in Fig. 6. The distribution is narrow and symmetric with no pronounced tailing. The peak value is 13 mK which is a reduction of √8 relative to the single frame value. This is as expected for pure shot noise, and shows that any noise introduced by the averaging procedure is negligible.

Figure 7 shows a map of the pixel QE for the same FPA as in Fig. 6, in which none of the defective pixels have been

Figure 6. NETD distribution of the Pelican-D LW FPA at 77K and at a frame rate of 30 Hz.

removed. The total number of both hard and soft defects on the FPA, defined according to SCD's stringent production line criteria, is 1446 giving an FPA operability of 99.56 per cent in this case. The QE values for each pixel are the average values over the usable LWIR spectral window, defined as the number of photoelectrons measured by the ROIC divided by the number of photons arriving from a black body at 35 °C in the spectral range 8.0 µm (cold filter cut-on value) to the detector cut-off wavelength. The QE map in Fig. 7 shows an almost constant value of ~ 48 per cent across the whole FPA, which agrees quite well with the value expected for a one pass detector with the same AL thickness (4.5 µm) discussed in section 2. If we define the background limited performance (BLIP) temperature as the detector operating temperature at which the dark current is equal to the photocurrent, the QE and dark current results discussed in this section yield a BLIP temperature of 87 K for a single pass Pelican-D LW FPA with F/2.7 optics. This is significantly higher than the operating temperature of 77 K. At 77 K, the dark current is more than 10× smaller than the photocurrent and as noted above, its distribution is narrow, making for good image stability against small temperature fluctuations.
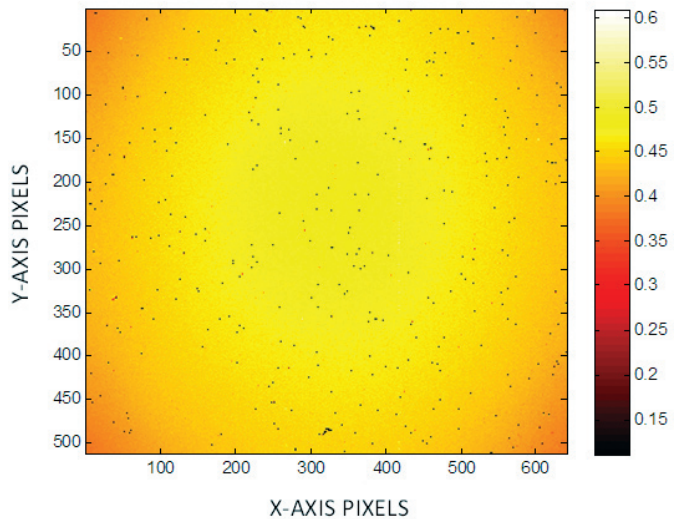

Figure 7. QE Map of the Pelican-D LW FPA operating at 77 K.

Finally, in Fig. 8, we show an image of a scene at 5 km registered with the Pelican-D LW FPA operating at 77 K, and in Table 2 the current performance specifications is listed.

Figure 8. Image registered with the 15µm pitch, 640 × 512 Pelican-D LW FPA operating with F/2.7 optics at 77K (Scene distance = 5 Km).

Table 2. Specification of performance of Pelican-D LW IDCA at 77 K

Parameter	Value
Format	640 × 512
Pitch	15 µm
Cut-off wavelength	9.3µm (filter)
Quantum efficiency	> 50 per cent
Operability	> 99 per cent
RNU	< 0.04 per cent STD/DR @ 10 -90 per cent Well Fill capacity
NETD	15 mK @ 65 per cent Well Fill capacity, 30 Hz (by averaging 8 frames)
Response uniformity	< 2.5 per cent (STD/DR)
Electronics	Camera Link
Cooler	Ricor K548
Weight	750 gm
Environmental conditions	-40 °C to +71 °C
Total power at 23 °C	16 W
Cool down time	8 min
MTTF (depends on mission profile)	15,000 h

5. CONCLUSIONS

In this study Pelican-D LW, which is SCD's new LWIR FPA detector is presented. It has a format of 640 × 512 with a 15 µm pitch, and operates at 77 K with a nominal detector cut-off wavelength, defined currently by a cold filter, of 9.3µm. The pixel operability is above 99 per cent, according to SCD's standard production line criteria for the definition of bad pixels. The present version is a single pass detector with a QE of ~48 per cent and exhibits very high uniformity and stability of its response and dark current. The FPA has a very stable

RNU below 0.02 per cent of the dynamic range (DR) for well fills between 40 per cent and 80 per cent. The active sensing material is based on a patented diffusion limited XB_pp barrier architecture, where an InAs/GaSb T2SL is used for the AL and an InAs/AlSb T2SL is used for the barrier layer. We have shown that sophisticated simulation techniques exist at SCD which can predict the detector cut-off wavelength and spectral response a-priori, according to the individual layer thicknesses chosen for each superlattice period, and the overall active layer stack thickness. Pelican-D LW demonstrates the versatility of InAs/GaSb as a tunable active layer detector material, and shows that this material can now be considered to be a realistic alternative to $Hg_xCd_{1-x}Te$ for small pitch, high performance LWIR and dual-color FPA detectors

REFERENCES

1. Glozman, A.; Harush, E.; Jacobsohn, E.; Klin, O.; Klipstein, P.C.; Markovitz, T.; Nahum, V.; Saguy, E.; Oiknine-Schlesinger, J.; Shtrichman, I.; Yassen, M.; Yofis, B. & Weiss, E. High performance InAlSb MWIR detectors operating at 100 K and beyond. *In* Proc. SPIE **6206**, 2006. article 6206-0M.

2. Klipstein, P.C. Depletionless photodiode with suppressed dark current. US Patent 7,795,640, 2 July 2003.

3. Klipstein, P.C. Unipolar semiconductor photodetector with suppressed dark current. US Patent 8,004,012, 6 April 2006.

4. Klipstein, P.C.; Aronov, D.; Berkowicz, E.; Fraenkel, R.; Glozman, A.; Grossman, S.; Klin, O.; Lukomsky, I.; Shtrichman, I.; Snapi, N.; Yassen, M. & Weiss, E. New "bariode" device reduces cooling requirements of infrared detectors. *In* SPIE Newsroom, November 2011

5. Tennant, W.E. Rule 07 revisited: Still a good heuristic predictor of p/n HgCdTe photodiode performance? *J. Elect. Mat.*, 2010, **39**, 1030.

6. Klipstein, P.C.; Avnon, E.; Benny, Y.; Fraenkel, R.; Glozman, A.; Grossman, S.; Klin, O.; Langoff, L.; Livneh, Y.; Lukomsky, I.; Nitzani, M.; Shkedy, L.; Shtrichman, I.; Snapi, N.; Tuito, A. & Weiss, E., InAs/GaSb Type II superlattice barrier devices with a low dark current and a high-quantum efficiency. *In* Proc. SPIE **9070**, 2014, article 9070-0U.

7. Klipstein, P.C.; Livneh, Y.; Glozman, A.; Grossman, S.; Klin, O.; Snapi, N. & Weiss, E. Modeling InAs/GaSb and InAs/InAsSb superlattice infrared detectors. *J. Elect. Mat.*, 2014, **43**, 2984

8. Livneh, Y.; Klipstein, P.C.; Klin, O.; Snapi, N.; Grossman, S.; Glozman, A. & Weiss, E., $\mathbf{k} \cdot \mathbf{p}$ model for the energy dispersions and absorption spectra of InAs/GaSb type-II superlattices. *Phys. Rev. B.* 2012, **86**, 235311; Erratum, *Phys. Rev. B*. 2014, **90**, 039903.

9. Klipstein, P.C.; Y Gross, Aronov, D.; Ben Ezra, M.; E Berkowicz, Cohen, Y.; Fraenkel, R.; Glozman, A.; Grossman, S.; Klin, O.; Lukomsky, I.; Markowitz, T.; Shkedy, L.; Shtrichman, I.; Snapi, N.; Tuito, A.; Yassen, M. & Weiss, E., Low SWaP MWIR detector based on XBn focal plane array. *In* Proc. SPIE **8704**, 2013, article 8704-1S

ACKNOWLEDGEMENTS

CONTRIBUTORS

Dr Philip Klipstein, received his BA and PhD in Physics from Oxford and Cambridge Universities respectively. After two years as a Junior Research Fellow at Cambridge, he moved to a tenured post at Imperial College, London. Research included transport and optics in GaAs/AlAs and Si/Ge. He joined Semiconductor Devices (SCD) in 2001. He is currently a Senior Scientist and Leading Researcher in the Antimonide Based Compound Semiconductor program (ABCS).

Contribution of contributors in the current study

P.C. Klipstein : Principal investigator and device design, performance simulation and data analysis.

I. Lukomsky, M. Nitzani, E. Avnon, L. Krasovitski : Device and FPA fabrication.

Y. Benny, A. Glozman, L. Langof, L. Shkedy : Device and FPA characterisation.

E. Hojman, O. Klin, N. Snapi, E. Weiss : Crystal growth.

E. Ilan, R. Talmor, S. Vaserman : Electronics and read out integrated circuit (ROIC) design.

E. Kahanov : Dewar design and mechanics.

A. Fraenkel, I. Shtrichman, A. Tuito : System design.